MJFAS
Malaysian Journal of Fundamental and Applied Sciences

Ashiru *et al*. | Malaysian Journal of Fundamental and Applied Sciences, Vol. 17 (2021) 647-658

RESEARCH ARTICLE

Highly Stable Photocatalytic Removal of Paraquat Dichloride using ZnO/TiO_2 supported on PVC

Abubakar Garba Ashiru[a,b], Juan Matmin[a], Susilawati Toemen[a,*]

[a] Department of Chemistry, University Teknologi Malaysia, 81310, Skudai, Johor Bahru, Malaysia; [b] Department of Chemistry, Zamfara State College of Education, PMB 1002, Maru, Zamfara State, Nigeria

Abstract This study presents on ZnO/TiO_2 supported on PVC (ZnO/TiO_2@PVC) in the photocatalytic removal of paraquat dichloride. The ZnO/TiO_2@PVC was characterized using XRD, FESEM-EDX, FTIR, and AFM. Findings indicated that ZnO/TiO_2@PVC allowed degradation of paraquat dichloride under UV irradiation by the rate of up to 73%. XRD pattern indicated the presence of both TiO_2 (anatase) and ZnO (zincite) crystalline as well as PVC amorphous structures. FESEM and AFM results revealed the observed shape and surface of TiO_2 interconnected nanowires with ZnO nanorods uniformly distributed according to EDX mapping. The reduced surface roughness was also shown in the supported photocatalyst. FTIR analysis clearly demonstrate the combined spectra of immobilised ZnO/TiO_2 powder catalyst onto the PVC in the composite. Kinetic study of the degradation process was performed according to pseudo-first-order and the influence of ZnO/TiO_2 coating onto PVC polymer and initial paraquat concentration were investigated on the treatment performance. Under optimized condition (pH = 7, PQ =20 mg/L and catalyst coating =15%), the stability and reusability of the supported catalyst was also evaluated over ten sequential treatment runs, and the catalyst maintain high reactivity. High recyclability of the ZnO/TiO_2@PVC composites as catalyst in photodegradation processes are also reported in this study.

Keywords: composite ZnO/TiO_2, supported nanostructures, paraquat dichloride, photocatalytic degradation.

Introduction

***For correspondence:** susilawatitoemen@utm.my

Received: 19 August 2021
Accepted: 14 October 2021

© Copyright Ashiru. This article is distributed under the terms of the Creative Commons Attribution License, which permits unrestricted use and redistribution provided that the original author and source are credited.

Organic polymers are considered as excellent substrates for photocatalytic removal based on TiO_2 nanostructure, which are typically prepared by sol–gel and hydrothermal synthesis [1]. The size, surface properties, and the reaction properties with active phase are also important factors that determine the activities of catalysts. The preparation processes of catalysts include bearing the active phases on the supports by the methods of impregnation, sol-gel, hydrothermal, and co-precipitation, drying, and calcination [2]. Drying is used to remove the water molecules that are physically adsorbed on the catalysts. Calcination is used to promote the formations of metal oxides and increase the combination strength between the active phases and supports. Calcination at different temperatures changes the surface properties of catalysts (such as surface areas and porosities) and the crystalline types of support (γ-Al2O_3 becomes α-Al2O_3 at high temperature) [3]. The solvent used in the binding of the support with the catalyst also play a very important role in the support material [4].

To increase the reusability of TiO_2-catalysts, supported materials such as alumina, silica, zeolites, and

activated carbon had been introduced [5, 6]. Notably, the selection of supported materials is not straightforward. There are several properties to consider when selecting the support materials such as (1) cycle life of the supported catalysts (2) solvent and binder (3) distribution of the catalyst on the support material (4) beneficial catalytic activities, and (5) avoiding nanocrystalline deterioration [7]. For stable photocatalysis applications, the preparation of inorganic polymers composites is currently attracting significant attention. This includes the immobilization of semiconductors on poly (methyl methacrylate) (PMMA) [8], polycarbonate (PC) [9], polystyrene (PS) [10], polyamide (PA) [11], polyethylene (PE) [12] or polyethylene terephthalate (PET) [13].

On the other hand, wastewater contamination has been a serious challenge of the environment for decades and needs innovative approach. In recent decades, remarkable population growth has led to a rapid enhancement in the agricultural production and use of agrochemicals which led to generation of wastewater in underground and surface water. Among the contaminants, herbicide paraquat dichloride which composed of a wide range of toxic and hazardous compounds such as refractory organic substances, dissolved solid particles, ammonia-nitrogen, and chloride. Recently, there has been a growing interest in application of heterogeneous metal oxides catalysts for the degradation of organic pollutants. Moreover, several studies have been carried out on organic pollutants degradation via ZnO/TiO_2 as catalysts. Most recently, the application of heterogeneous catalytic degradation processes for paraquat dichloride has been focused on providing support and recovery [14]. Accordingly, performance of prepared bimetallic ZnO/TiO_2 as a heterogeneous catalyst was examined in the aqueous solution system, and high degradation efficiency was achieved [15].

In this study, we report the surface coating of ZnO/TiO_2 photocatalyst on organic substrates of polyvinyl chloride. Mechanochemical method was proposed for synthesis of heterogeneous ZnO/TiO_2 nanostructured catalyst and implemented for degradation of paraquat dichloride. The mono metal oxides of ZnO and TiO_2 catalysts were prepared by facile sol-gel/hydrothermal method. The bimetallic supported catalyst was prepared by simple chemical deposition method. Physicochemical properties of the catalysts were characterized by XRD, FESEM-EDX, FTIR and AFM analytical techniques. The activity and kinetics of photodegradation of paraquat via $PVC@ZnO/TiO_2$ catalyst was illustrated and used for interpreting the performance of the catalysts for degradation process at optimum conditions. The influence of different operating parameters such as catalyst loading, pollutant concentration, and co-catalyst ratio was also investigated on photocatalytic activity of the PQ. Furthermore, the stability and recyclability of the synthesized supported and unsupported catalysts were examined during ten repeated cycles of treatment at best selected conditions.

Materials and methods

Chemicals

Titanium tetraisopropoxide ($C1_8H_{28}O_4Ti$, 97%, Sigma-Aldrich), zinc acetate dihydrate ($Zn(CH_3COO)_2.2H_2O$, 99.9%, QReC), Polyvinyl chloride (Sigma Aldrich), sodium hydroxide (NaOH, 98%, QReC), and hydrochloric acid (HCl, 37%, QReC) were purchased from VNK Supply & Services. The Tetrahydrofuran (THF) organic solvent was purchased from Merck. A surfactant of cetyltrimethylammonium bromide ($C_{19}H_{42}BrN$, 97%, Sigma-Aldrich) was provided from Merck. For the photodegradation test, a herbicide type of paraquat dichloride ($C_{12}H_{14}C_{l2}N_2$, 99%, Sigma-Aldrich) was supplied by Sigma Aldrich.

Synthesis of Photocatalysts

Synthesis of Bimetallic Unsupported ZnO/TiO_2 Photocatalyst

To synthesize the TiO_2 nanostructures a weighed amount of titanium tetraisopropoxide (TTIP) was dissolved with 150 mL of ethanol, before dropwise addition of 1 mL of water. The mixtures turned to a milky solution after 30 min of stirring and followed by addition of 0.5 mL HNO_3. The solution was kept at room temperature for overnight and followed by drying in an oven at 75 ^oC for 48 h. Next, the dried solids were calcined at 500 ^oC for 2 h. Subsequently, the calcined solids were treated with 10 M NaOH and transferred into Teflon-lined autoclave before heated at 150 ^oC for 18 h. Considerable amounts of white

powders were collected by allowing the autoclave to cool at room temperature and consecutively washed until the ~pH 7 before stored to dry for overnight. After drying, the powder was calcined at 500 °C for 2 h to give opal-white powder and labelled as TiNW. The second step was the synthesis of ZnO nanorod. Simply, a weighed amount of zinc acetate dihydrate was dissolved in 60 mL of distilled water, before dropwise addition of 25 mmol of cetyltrimethylammonium bromide in 1 mol of KOH. The mixtures were stirred for 1 h to give a cloudy solution. Later, the precipitates were collected, transferred into a stainless-steel autoclave, and heated at 120 ^{o}C for 5 h. Afterwards, the solids were collected and consecutively washed until the ~pH 7 before stored to dry for overnight. After drying, the powder was calcined at 900 ^{o}C for 2 h to give white powder and labelled as ZnNR. Finally, to prepare the ZnNR/TiNW nanostructures, an appropriate amount of TiNW and ZnNR were mixed in a container under constant shaking. After a while, the solid mixtures were subjected to Planetary Ball Mill PM 100 (Retsch, Germany) using a high-energy. The ball milling was operated at 400 rpm for 1 h with the mass ratio of balls to powder at 1:1 in an air medium. The final fabricated products resulted in white powder and were labelled according to the wt.% of ZnNR loadings as ZnNR/TiNW.

Preparation of PVC Supported ZnO/TiO$_2$

1g of polyvinyl chloride (PVC) powder was slowly dissolved in 25 mL of tetahydrofuran (THF) solution under vigorous stirring. The obtained clear solution was then poured onto a Petri dish and left for 10 min till the solution starts to solidify. The prepared photocatalyst was spread on top of the semi-solid PVC layer and left overnight to dry. It should to be noted that the formation of semi-solid PVC layer is very important as over-drying would lead to leaching of the catalyst as the catalyst would not be completely held on the film. The dried composite was further dried at 95 °C for 1 h to remove any moisture [7, 16]. The prepared composite was labelled as PVC@ZnNR/TiNW.

Characterization Methods

The X-ray powder diffraction (XRD) patterns were collected on SmartLab XRD (Rigaku, Japan) using CuKα radiation (1.54 Å). D-spacing was calculated using Equation 1 expressions as follows.

$$\lambda = 2\, d \sin\theta \quad (1)$$

Where λ is the wavelength of the incoming X-ray beam and dhkl is the interplanar spacing of a plane with normal hkl. Accordingly, Debye-Scherrer Equation was used for the calculation of average crystal size according to the following expressions:

$$D = (0.9\,\lambda)/(\beta \cos\theta) \quad (2)$$

where D is the size of the crystal, λ is the wavelength of the X-ray, θ is Braggs angle (in radians), and β is full width at half maximum (in radians) of a peak. Field emission scanning electron microscopy (FESEM) images were retrieved using the JEM-2100 F FESEM (JEOL, USA) coupled with XMax 80 T (Oxford) detector for simultaneous elemental composition determination using electron dispersive X-ray (EDX) analysis. The chemical bonding and functional groups information of the samples were obtained using a Nicolet iS10 (Thermo Fisher Scientific, USA) on an attenuated total reflectance-Fourier transform infrared (ATR-FTIR) spectrophotometer. In the photocatalytic experiments, the absorbance changes in wavelength from 200 to 800 nm were monitored using UV-Visible Lambda 25 spectrophotometer (Perkin Elmer, USA). The AFM analysis was conducted using NanoWizard® 3 Atomic Force Microscope (JPK Instruments).

Photocatalytic Activity

The photocatalytic activity of all samples was assessed by their ability to degrade the aqueous solution of paraquat dichloride. In this experiment, 80 mg of each sample was suspended in 200 mL of 20 ppm paraquat dichloride aqueous solution. The reaction was performed in a photoreactor equipped with UVP Black-Ray J-221 (0.60 mW/cm^2) of a UV lamp (Analytik Jena, USA) as the irradiation source. Prior to UV irradiation, the mixture was poured into a glass beaker and stored in a dark environment under continuous stirring for 30 min to achieve an equilibrium adsorption-desorption state. After every 60 min,

3 mL of the mixture was withdrawn, separated from the solid suspensions by a centrifuge, and analyse using UV-Visible spectrophotometer. The UV-Vis monitoring was conducted for 4 h and the residual concentration of paraquat dichloride was determined at the absorbance wavelength of 257 nm. The photodegradation activity was evaluated by using Equation 3 [17, 18]:

$$\text{Photodegradation (\%)} = (C_o\text{-}C_t)/C_o \quad \text{x } 100 \tag{3}$$

where C_o is the initial concentration, while C is the final concentration after the photodegradation.

Results and discussion

Characterizations

XRD

The XRD diffraction patterns of the ZnNR/TiNW, PVC@ZnNR/TiNW, and that of pristine PVC was compared as shown in Figure 1a. Based on Figure 1a, it can be seen from the diffractogram that the unsupported and supported photocatalysts are compared and the peaks from the 5-ZnNRTiNW clearly matched those in the PVC@ZnNR/TiNW. For TiO_2, the characteristic peaks at 2θ values of 25.39º, 37.72º, 48.27º, 53.86º, and 55.32º corresponding to (101), (004), (200), (105), and (211) planes. The crystal structure is in good agreement with the ICCD #21-1272. For ZnO (ICDD# 36-1451), the peaks at 2θ values of 31.89º, 34.79º, 36.45º, 56.83º, 63.47º, and 68.39º corresponding to (100), (002), (101), (110), (103), and (112) respectively. It can be observed in Figure 1a that the spectrum of the bare PVC did not show any sharp peak, with the patterns exhibiting an amorphous background emanating mainly from the polymer amorphous phase [19] indicating the amorphous structure of PVC (shown in the inset), while XRD scan of PVC@ZnNR/TiNW films having 15 wt.%, (Figure 1a) indicated sharp peaks related to ZnNR and TiNW and amorphous regions of PVC at 2θ = 24.61°. In details, the following 2θ values were identified for the amorphous PVC (1,1,2-trichloroethane) 19.50º, 24.61º, 27.14º, 31.33º, and 31.90º which are assigned to (110), (11-2), (12-1), (031), and (004) planes, respectively. This was an evidence that ZnNR/TiNW bimetallic composite were incorporated in PVC matrix with no changes in the wurtzite crystal-like, and anatase structure of ZnO and TiO_2, respectively. Notably, the crystallinity of polyethene materials is very low, its reflection peaks therefore did not appear obviously. These results were consistent to Sadek et al. [20] and Hasan et al. [21] on incorporating ZnO and TiO_2 nanostructures PVC matrix. Meanwhile the average crystallite size of the ZnO/TiO_2 supported bimetallic composite samples calculated using the Debye-Scherrer's Equation (1) is ~15 nm.

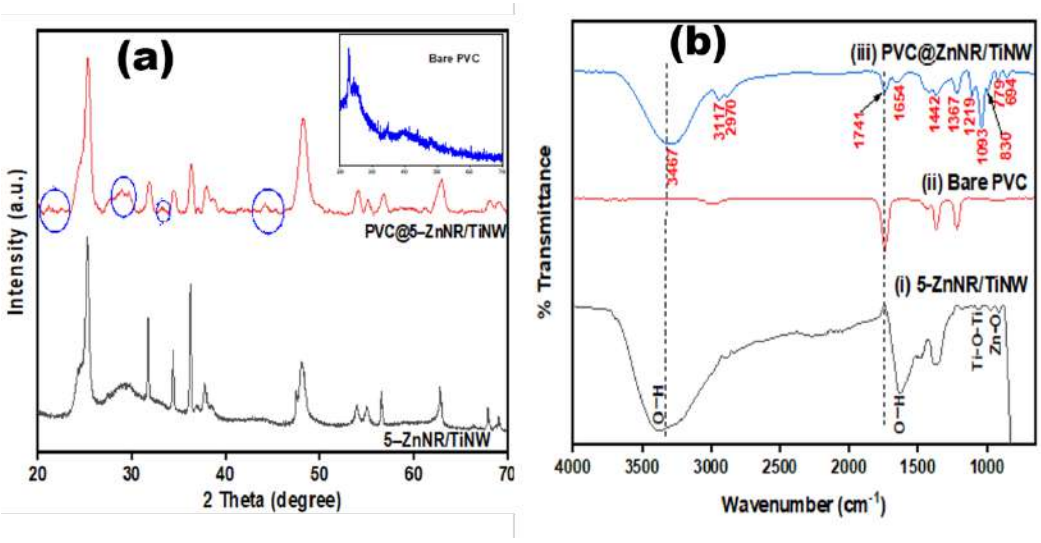

Figure 1. (a) XRD and (b) ATR-FTIR spectra of PVC supported ZnNR/TiNW compared with unsupported, and with bare PVC (inset)

FTIR

Fourier infrared spectra measurement was conducted on the solid samples using ATR. Comparison was also made with the unsupported catalyst to demonstrate the immobilization of the bimetallic photocatalyst on the PVC thin film. Figure 1b shows the ATR-FTIR spectra of ZnNR/TiNW (Figure 1b(i)), bare PVC (Figure 1b(ii)), and PVC@ZnNR/TiNW (Figure 1b(iii)). The supported photocatalyst clearly demonstrate the combine spectra of the immobilized powder catalyst onto the polyvinyl chloride and confirmed the presence of ZnO/TiO_2 and the PVC composites [22]. The characteristic stretching vibrations of the Ti–O–Ti inorganic network are present in the composite samples between range of 400 and 800 cm^{-1} and are attributed to O–Ti–O from crystalline anatase titania form [23]. Typical vibrational bands of T–O−T are observed at 964 and 830 cm^{-1} attributed to TiO_2, and for ZnO, the vibrational band at 694 cm^{-1} confirms the presence of Zn–O bond. Previous works reported that bands below 1000 cm^{-1} are associated with the stretching vibration mode M–O owing to the formation of metal oxides [24]. For the PVC@ZnNR/TiNW composite, the C–Cl stretch corresponding to chlorine content in PVC was identified at a vibration band of 899 cm^{-1} [25]. The appearance of 1367 and 1219 cm^{-1} peaks indicate the presence of in-plane CH_2 deformation of PVC, and of C–O bond, respectively [26]. The vibrational bands attributed to the C–H bonds of the aromatic rings are discernible in the range 3100–2800 cm^{-1}, while the peak at 1093 cm^{-1} is assigned to C–C of the aliphatic hydrocarbons in the polymer. The peaks at 1654 and 3467 cm^{-1} are attributed to the O–H group of the surface and adsorbed water molecule in the samples. The peaks at 1093 and 779 cm-1 are attributed to tras C–H and cis C–H wagging, respectively. Similar results were reported by Ramesh et al. [27].

FESEM-EDX

Figure 2 depicts the FESEM micrographs of unsupported and PVC supported ZnNR/TiNW bimetallic composites. In the case of PVC@ZnNR/TiNW, almost regular distribution of ZnO, and TiO_2 nanostructure at 15 wt.% in PVC matrix can be clearly observed in Fig. 2b. Moreover, the wire-like structure of TiO_2 and the rod-like ZnO nanostructures can be clearly seen. The field emission scanning electron microscopy (FESEM) analysis was used for observing the polymer coated surface [28]. By comparison of Fig. 2a and 2b, it can be demonstrated that ZnO/TiO_2 nanostructures were successfully immobilized on the surface of PVC. Mixed particles of interconnected TiO_2 nanowires with ZnO nanorods attached and uniformly distributed in the TiO_2 matrix can be clearly seen. Figure 2b (inset) illustrates the FESEM image of the PVC film before coating at high magnification. The results of FESEM analysis were in agreement with previous studies [29, 30]. The energy dispersive X-ray (EDX) technique was utilized to analyze the elemental composition of PVC films with bimetallic ZnNR/TiNW coated after the UV irradiation. Figure 2c shows the elements and EDX images of PVC supported photocatalyst that demonstrated the bimetallic powder samples were well dispersed and mixed on the polymer materials [31]. The weight % composition of the Ti, Zn, O, C, and Cl elements are 28.6, 1.3, 22.3, 44.2, and 3.7%, respectively which matched well with the 5:95 ratio of the 15% metal oxides coated on the PVC polymer materials.

EDX Mapping

EDX images of supported PVC@ZnNR/TiNW are shown in Fig. 3. Based on the images of the Ti, Zn, O, C, and Cl elements, the presence of ZnO, TiO_2 and PVC $(C_2H_3Cl)_n$ on the surface of PVC was proved. Fig. 3a-c show the distribution of Ti, Zn, and O respectively which are the elemental content of the ZnNR/TiNW photocatalyst and can be identified with the wt.% of 28.6 (green), 1.3 (orange), and 22.3% (purple) for Ti, Zn and O, respectively. The carbon and chlorine in PVC can be identified with red and blue colors having 44 and 3.7 wt.%, respectively (Fig. 3e, f). The EDX layered image (Fig 3f) indicated the total distributions according to the elemental composition of the PVC@ZnNR/TiNW photocatalyst. It can be clearly observed that Ti dominates the highest region with only few regions occupied by Zn, O, and Cl. Notably, the blue color representing the carbon in PVC cannot be seen as its covered by the coated ZnNR/TiNW material.

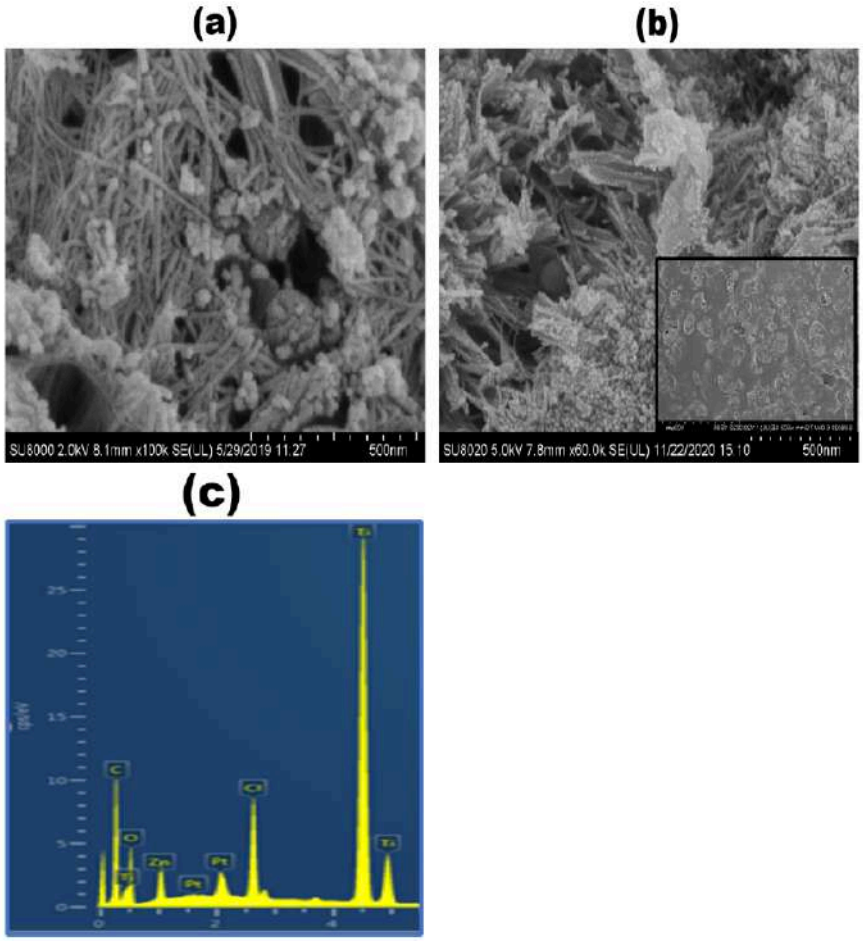

Figure 2. FESEM images of (a) ZnNR/TiNW and (b) micrograph, and (c) EDX pattern of PVC@ ZnNR/TiNW

AFM

Figure 3g-h represents the two and three-dimensional images of the surface of PVC film surface coated with 0.2 g ZnNR/TiNW photocatalyst. The surface roughness is shown by the image in Figure 3g and the root-mean-square roughness (Rrms) value of the photocatalyst loading is 6.24 nm. The low Rrms value proves the reduction in the amount of catalyst exposed on surface [32]. Thus, the decrease in number of catalyst particles on PVC surface can lead to reduction of the adsorbed UV light intensity. Moreover, the contact between photocatalyst and pollutant also become less and can cause the decrease in the activity as compared to the powdered catalyst which has sufficient contact during the reaction. In general, the AFM images of the PVC supported photocatalyst show non-homogeneous surfaces with some agglomerated particles and scratches (like hill-chains aspect). Figure 3h clearly shows the formation of mainly bigger particles of oxides containing ZnO nanorods. This also supports the fact of the existence of well separated polycrystalline phases in the layer [1, 16, 19].

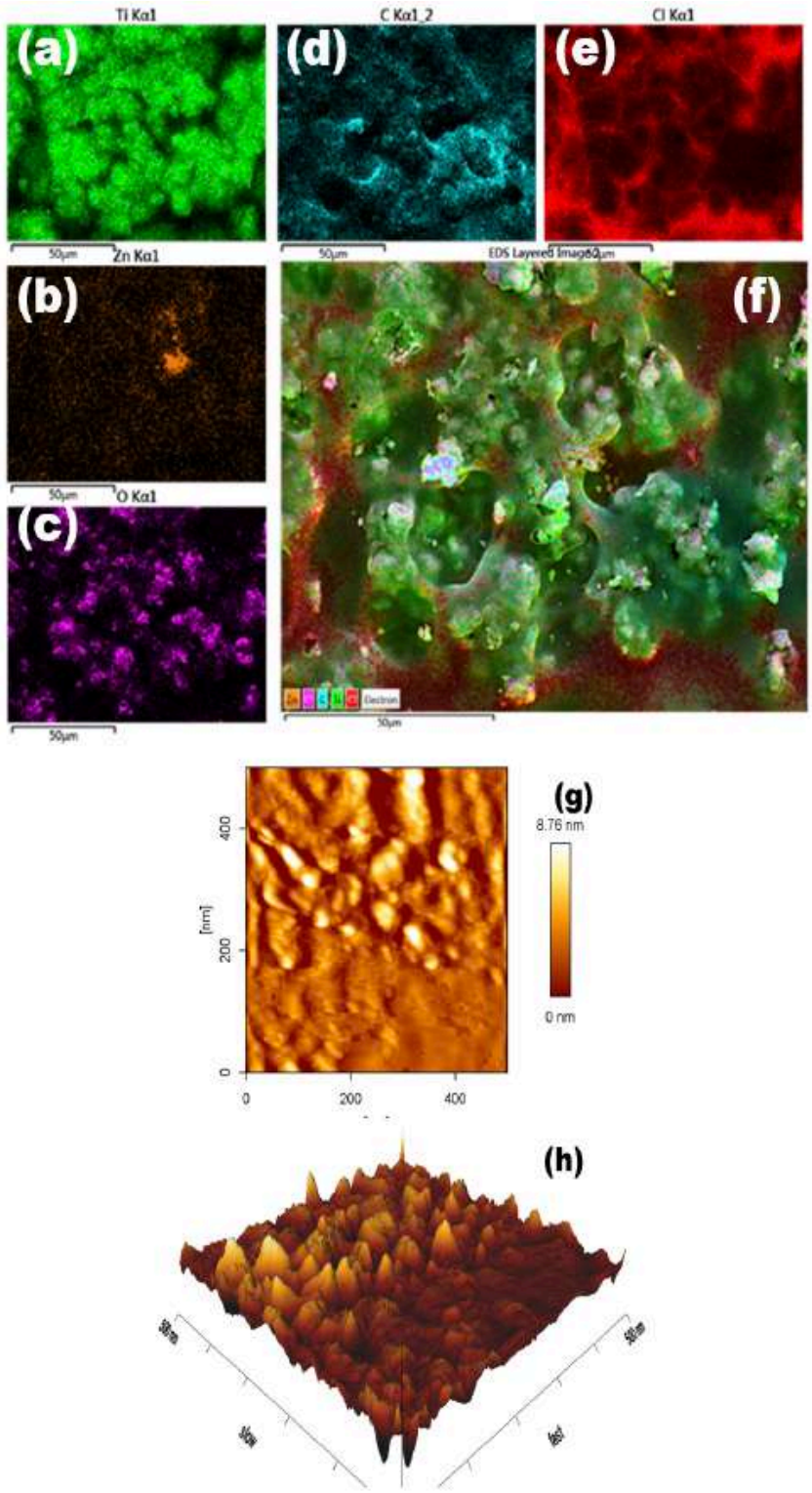

Figure 3. EDX Mapping of FESEM micrographs for elemental distribution of (a) Ti (b) Zn (c) O (d) C (e) Cl, and (f) PVC@ZnNR/TiNW and AFM image of 0.8 g/L PVC@ZnNR/TiNW (g) 2D and (h) 3D

Photocatalytic Activity

Supported and unsupported (powdered) photocatalysts were compared to investigate their efficiencies towards degradation of paraquat. Further, this study also investigated the reusability of the supported photocatalyst on the degradation of paraquat dichloride for large scale application. Figure 4 shows the plot of percentage degradation against the time of the supported and unsupported samples. As can be observed, the powdered (unsupported) ZnNR/TiNW shows higher degradation than supported PVC@ZnNR/TiNW with 82.75, and 73.33%, respectively in the percentage degradation of paraquat dichloride. The reason for the low performance of the supported might be due to the reduced surface and trap in the number of active sites by the PVC polymer that reduced the % degradation by ~10%.

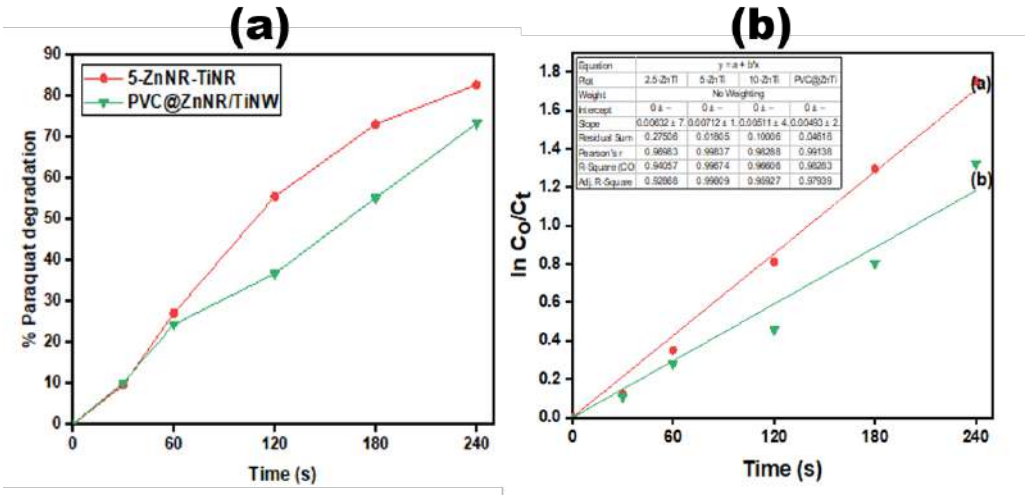

Figure 4. (a) Photocatalytic degradation (%) of paraquat dichloride under UV light irradiation, over unsupported ZnNR/TiNW and supported PVC@ZnNR/TiNW, and (b) Kinetic Linear Fit of paraquat photocatalytic degradation under UV irradiation, of unsupported compared with PVC supported ZnNR/TiNW

Kinetics

Figure 4b shows the linear plot of ln C_o/C_t against time for the degradation of paraquat dichloride. The linear relationship also indicates that the photodegradation mechanism followed the pseudo-first-order kinetics and is similar to photodegradation of common herbicides such as atrazine [33], bentazon [34, 35], carbaryl [36], triazinone [37], and 2,4-dichlorophenoxyacetic acid [38, 39]. During the first 600 min of the degradation experiment, the photocatalytic performance of both the unsupported and supported samples progress in the same rate. However, the ZnNR/TiNW nanostructures maintain higher due to stable photogeneration of e^- and h^+. Table 2 present the rate constant (k), half-life ($t_{1/2}$), and percentage degradation (%) for unsupported and supported samples. The k values for ZnNR/TiNW and PVC@ZnNR/TiNW are, 7.50 x 10^{-3} and 5.26 x 10^{-3}, respectively. Remarkably, the calculated $t_{1/2}$ value for the ZnNR/TiNW was 93 min indicating rapid photodegradation reaction as compared to the supported (132 min) and work done by others [3, 10]. Based on the findings, it is, therefore, suggested that ZnNR/TiNW nanostructures have the most photogenerated radicals that are useful on the catalyst surfaces to enhanced degradation activity compared to the supported PVC@ZnNR/TiNW. To compare the catalytic activity with other nanostructured materials, the photodegradation of paraquat obtained from this method is also higher than Kanchanatip et al. (70%), [40] and Trovo et al. (66.6%) [41] as reported in Table 1.

Table 1. The rate constant (k), half-life ($t_{1/2}$), and percentage degradation (%) of synthesized samples

Sample	Rate constant, k (min^{-1})	Half-life, $t_{1/2}$ (min)	Percentage degradation (%)
ZnNR/TiNW	7.50×10^{-3}	93	82.75
PVC@ZnNR/TiNW	5.26×10^{-3}	132	73.33
C_{60}/V-TiO_2 [40]	1.71×10^{-1}	4	70
Fe^{2+}/H_2O_2 [41]	-	-	64.6

Reusability Studies of PVC@ZnNR/TiNW for Paraquat Degradation

The reusability of the photocatalyst was also evaluated by carrying out series of photocatalytic reactions using the supported PVC@ZnNR/TiNW and compared with the unsupported powder catalyst. Figure 5a shows the experimental runs with the photocatalyst over the sequential treatment. The supported catalyst showed high reactivity over ten repeated cycles carried out with the PVC@ZnNR/TiNW samples as the representative photocatalyst under UV light irradiation. While the powdered ZnNR/TiNW catalyst attain it deactivation point after the sixth run with a decreased activity of ~5%. There was a slight decrease (~5%) in paraquat degradation efficiency after the first cycle in the case of the supported catalyst. The results demonstrate that after repeated degradation use, only ~5% decrease in photocatalytic degradation efficiency can be observed, indicating good stability of the PVC@ZnNR/TiNW supported photocatalyst [42].

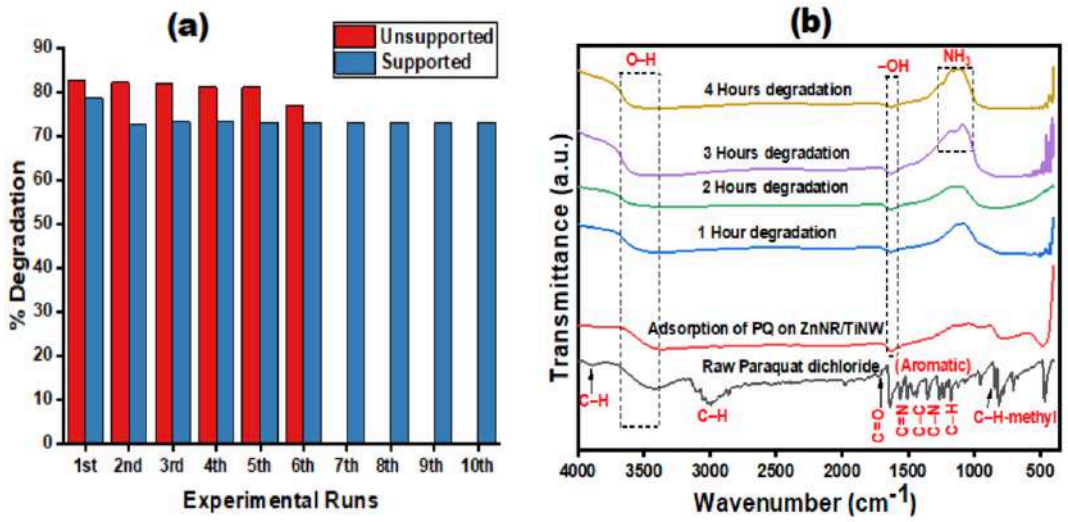

Figure 5. (a) Experimental runs for degradation of paraquat over unsupported and PVC supported ZnNR/TiNW, and (b) ATR-FTIR spectra of degradation process of paraquat dichloride over supported and unsupported ZnO/TiO2 photocatalysts

ATR-FTIR Analysis of Degraded Products

To prove the capability of the treatment process in paraquat dichloride degradation, comparison of functional groups using ATR-FTIR analysis of the paraquat samples before and after the degradation process was conducted. The degradation products were studies and the results showed that aromatic compounds in the paraquat were converted to aliphatic components after the degradation. Figure 5b represents the FTIR spectra of the unsupported, supported, and the degradation products of 4 hour at different time interval. It can be observed in Figure 5b that the spectra of the initial and degraded paraquat solution matched in the region of 4000 to 2000 cm-1. The peaks below 2000 cm-1 shown at 1734, 1370, and 1212 cm-1 appeared at 1 hour degradation and keep increasing up to 4 hours' time. Similar observation was reported by Karimipourfard, et al. for the degradation of leachate samples [43]. Meanwhile, after 4 h degradation, only transmittance peaks around 3600, 1600, and 1200 cm-1 attributed to OH groups and C=O, and N≡H of final degradation product of H2O, CO2 and NH3 are retained. The

analysis of the ATR-FTIR results showed that the PVC@ZnNR/TiNW composite was a promising catalyst in paraquat dichloride degradation.

Conclusions

In this study, ZnNR/TiNW@PVC was successfully prepared by hydrothermal/surface coating, and directly used in photocatalytic removal of paraquat dichloride in water system. Effect of parameters like paraquat initial solution, ZnO wt.% ratio and catalyst loading were investigated for the optimum efficiency of the process. The highest photocatalytic efficacy of the unsupported catalyst system was 83% which was attributed to 20 ppm paraquat initial solution, ZnO 5 wt.% ratio of and catalyst loading of 0.8 g/L. At the optimized condition, performance of the supported catalyst (73.33%) was also compared with performances of the unsupported 5-ZnO wt.% having degradation of 83%. These data demonstrated that the proposed PVC@ZnNR/TiNW bimetallic system showed decrease in performance compared to the unsupported ZnNNR/TiNW, this is due to the reduction the number of defects and active sites on the surface of the coated catalyst. Interestingly, after ten times reusability experiment, the supported photocatalyst proved to be more stable than the unsupported which deactivated at the sixth run. Furthermore, ATR-FTIR analysis performed on the paraquat solution samples before and after the photocatalytic process confirmed the presence of expected by-products in the treated samples. The results showed that aromatic compounds were converted to aliphatic components after degradation. From the results obtained, it could be concluded that the paraquat dichloride photocatalytic system treated by the supported bimetallic ZnO/TiO2 is promising in polluted water environmental remediation.

Data availability

Data are available on request.

Conflicts of interest

The authors declares that there is no conflict of interest regarding the publication of this paper.

Funding statement

This work was supported by the Ministry of Higher Education Malaysia for FRGS/1/2018/STG(01)/UTM/02/3 (5F076) and Universiti Teknologi Malaysia for UTM-ER PY/2019/01177 (18J18), UTM-FR PY/2019/01760 (21H03) and AST&D of Nigerian Tertiary Education Trust Fund (TETFund) 2017 Intervention.

Acknowledgments

This research is done with the support from Universiti Teknologi Malaysia and the Malaysia Ministry of Higher Education (MOHE). The authors would like to thank the University and the grant for providing the sponsorship.

References

[1] R. M. Cámara, E. Crespo, R. Portela et al., “Enhanced photocatalytic activity of TiO_2 thin films on plasma-pretreated organic polymers,” Catalysis Today, vol. 1, no. 230, pp 145–151, 2014.

[2] B. Srikanth, R. Goutham, R. B. Narayan et al., “Recent advancements in supporting materials for immobilised photocatalytic applications in wastewater treatment,” Journal of environmental management, vol. 1, no. 200, pp. 60–78, 2017.

[3] R. Linacero, M. L. Rojas-Cervantes, and J. D. Lopez-Gonzalez, “Preparation of $xTiO_2 \cdot (1-x)\ Al_2O_3$ catalytic supports by the sol-gel method: physical and structural characterization,” Journal of materials science, vol. 35, no. 13, pp. 3279–3287, 2000.

[4] M. Nawi and S. M. Zain, “Enhancing the surface properties of the immobilized Degussa P-25 TiO_2 for the efficient photocatalytic removal of methylene blue from aqueous solution,” Applied Surface Science, vol. 258, no. 16, pp. 6148–6157, 2012.

[5] K. Guesh, Á. Mayoral, Y. Chebude et al., "Effect of thermal treatment on the photocatalytic behavior of TiO_2 supported on zeolites," New Journal of Chemistry, vol. 42, no. 14, pp. 12001–12007, 2018.
[6] Y. Yang, S. H. Zhan, X. C. Gao et al., "Degradation of toluene using modified TiO_2 as photocatalysts," In Advanced Materials Research, vol. 669, pp. 7–18, 2013.
[7] S. Vankova, C. Francia, J. Amici et al., "Influence of Binders and Solvents on Stability of Ru/RuO_x Nanoparticles on ITO Nanocrystals as LiO_2 Battery Cathodes," Chemsuschem, vol. 10, no. 3, pp. 575–586, 2017.
[8] O. Ounas, A. A. El-Foulani, B. Lekhlif, and J. Jamal-Eddine, "Immobilization of TiO_2 into a poly methyl methacrylate (PMMA) as hybrid film for photocatalytic degradation of methylene blue," Materials Today Proceedings, vol. 22, pp. 35–40, 2020.
[9] D. K. Hwang, Y.-G. Shul, and K. Oh, "Photocatalytic Application of Au–TiO_2 Immobilized in Polycarbonate Film," Industrial & Engineering Chemistry Research, vol. 52, no. 50, pp. 17907–17912, 2013.
[10] R. Ata, O. Sacco, V. Vaiano et al., "Visible light active N-doped TiO_2 immobilized on polystyrene as efficient system for wastewater treatment," Journal of Photochemistry and Photobiology A: Chemistry, vol. 348, pp. 255–262, 2017.
[11] J. Shen, R. Steinbach, J. M. Tobin et al., "Photoactive and metal-free polyamide-based polymers for water and wastewater treatment under visible light irradiation," Applied Catalysis B: Environmental, vol. 193, pp. 226–233, 2016.
[12] J. Velásquez, S. Valencia, L. Rios, G. Restrepo, and J. Marín, "Characterization and photocatalytic evaluation of polypropylene and polyethylene pellets coated with P25 TiO_2 using the controlled-temperature embedding method," Chemical engineering journal, vol. 203, pp. 398–405, 2012.
[13] R. V. Aquino, A. A. Barbosa, L. B. Ribeiro et al., "Degradation of leaf green food dye by heterogeneous photocatalysis with TiO_2 over a polyethylene terephthalate plate," Chemical Papers, vol. 73, no. 10, pp. 2501–2512, 2019.
[14] A. Pourzad, H. R. Sobhi, M. Behbahani et al., "Efficient visible light-induced photocatalytic removal of paraquat using N-doped TiO_2@SiO_2@Fe_3O_4 nanocomposite," Journal of Molecular Liquids, vol. 299, pp. 112167, 2020.
[15] P. Nuengmatcha, S. Chanthai, R. Mahachai, and W. C. Oh, "Sonocatalytic performance of ZnO/graphene/TiO_2 nanocomposite for degradation of dye pollutants (methylene blue, texbrite BAC-L, texbrite BBU-L and texbrite NFW-L) under ultrasonic irradiation," Dyes and Pigments, vol. 134, pp. 487–497, 2016.
[16] R. Nadarajan, W. A. Bakar, R. Ali, and R. Ismail, "Method for polychlorinated biphenyls removal from mussels and its photocatalytic dichlorination," Applied Catalysis B: Environmental, vol. 218, pp. 327–337, 2017
[17] Y. Chang, C. Wu, H. Wang et al., "Effect of post-heat treatment on the photocatalytic activity of titanium dioxide nanowire membranes deposited on a Ti substrate," RSC advances, vol. 7, no. 35, pp. 21422–21429, 2017.
[18] L. Lu, R. Shan, Y. Shi, S. Wang, and H. Yuan, "A novel TiO_2/biochar composite catalysts for photocatalytic degradation of methyl orange" Chemosphere, vol. 222, pp. 391–398, 2019.
[19] E. García-Ramírez, M. Mondragon-Chaparro, and O. Zelaya-Angel, "Band gap coupling in photocatalytic activity in ZnO–TiO_2 thin films," Applied Physics A, vol. 108, no. 2, pp. 291–297, 2012.
[20] E. M. Sadek, N. A. Mansour, S. M. Ahmed, S. L. Abd-El-Messieh, and D. El-Komy, "Synthesis, characterization, and applications of poly (vinyl chloride) nanocomposites loaded with metal oxide nanoparticles," Polymer Bulletin, pp. 1–22, 2020.
[21] M. Hasan, A.N. Banerjee, and M. Lee, "Enhanced thermo-mechanical performance and strain-induced band gap reduction of TiO_2@PVC nanocomposite films," Bulletin of Materials Science, vol. 38, no. 2, pp. 283–290, 2015.
[22] T. Uma, T. Mahalingam, and U. Stimming, "Conductivity and thermal studies of solid polymer electrolytes prepared by blending polyvinylchloride, polymethylmethacrylate and lithium sulfate," Materials Chemistry and Physics, vol. 85, no. 1, pp. 131–136, 2004.
[23] D. X. Vargas, J. R. De la Rosa, C. J. Lucio-Ortiz et al., "Photocatalytic degradation of trichloroethylene in a continuous annular reactor using Cu-doped TiO_2 catalysts by sol–gel synthesis," Applied Catalysis B: Environmental, vol. 179, pp. 249–261, 2015.
[24] P. D. Shivaramu, A. Patil, M. Murthy, S Tubaki et al., "Magnetic substrate supported ZnO-CuO nanocomposite as reusable photo catalyst for the degradation of organic dye," Materials Today: Proceedings, vol 4, no. 11, pp. 12314–12320, 2017.
[25] D. Tabb and J. Koenig, "Fourier transform infrared study of plasticized and unplasticized poly (vinyl chloride)," Macromolecules, vol. 8, no. 6, pp. 929–934, 1975.
[26] A. Jagadeesan, M. Sasikumar, R. H. Krishna et al., "High electrochemical performance of nano TiO_2 ceramic filler incorporated PVC-PEMA composite gel polymer electrolyte for Li-ion battery applications," Materials Research Express, vol. 6, no. 10, pp. 105524, 2019.
[27] S. Ramesh, K. H. Leen, K. Kumutha, and A. K. Arof, "FTIR studies of PVC/PMMA blend based polymer electrolytes," Spectrochimica Acta Part A: Molecular and Biomolecular Spectroscopy, vol. 66, no. 4, pp. 1237–1242, 2007.
[28] X. Zhao, C. Peng, and J. You, "Plasma-Sprayed ZnO/TiO_2 Coatings with Enhanced Biological Performance," Journal of Thermal Spray Technology, vol. 26, no. 6, pp. 1301–1307, 2017.
[29] A. Behboudi, Y. Jafarzadeh, and R. Yegani, "Preparation and characterization of TiO_2 embedded PVC

ultrafiltration membranes," Chemical engineering research and design, vol. 114, pp. 96–107, 2016.
[30] T. Ahmad, C. Guria, and A. Mandal, "Synthesis, characterization, and performance studies of mixed-matrix poly (vinyl chloride)-bentonite ultrafiltration membrane for the treatment of saline oily wastewater," Process Safety and Environmental Protection, vol. 116, pp. 703–717, 2018.
[31] X. Wei, Z. Yang, S. L. Tay, and W. Gao, "Photocatalytic TiO_2 nanoparticles enhanced polymer antimicrobial coating," Applied surface science, vol. 290, pp. 274–279, 2014.
[32] B. I. Stefanov, G. A. Niklasson, C. G. Granqvist, and L. Österlund, "Gas-phase photocatalytic activity of sputter-deposited anatase TiO_2 films: Effect of <001> preferential orientation, surface temperature and humidity," Journal of Catalysis, vol. 335, pp. 187–196, 2016.
[33] M. Lackhoff and R. Niessner, "Photocatalytic atrazine degradation by synthetic minerals, atmospheric aerosols, and soil particles," Environmental science & technology, vol. 36, no. 24, pp. 5342–5347, 2002.
[34] M. Gholami, M Shirzad-Siboni, M. Farzadkia, and J. K. Yang, "Synthesis, characterization, and application of ZnO/TiO_2 nanocomposite for photocatalysis of a herbicide (Bentazon)," Desalination and water treatment, vol. 57, no. 29, pp. 13632–13644, 2016.
[35] M. Gholami, M Shirzad-Siboni, M. Farzadkia, and J. K. Yang, "Study of the decomposition and detoxification of the herbicide bentazon by heterogeneous photocatalysis: Kinetics, intermediates, and transformation pathways," Applied Catalysis B: Environmental, vol. 200, pp. 150–163, 2017.
[36] A. B. Prevot, E. Pramauro, and M. De la Guardian, "Photocatalytic degradation of carbaryl in aqueous TiO_2 suspensions containing surfactants, Chemosphere, vol. 39, no. 3, pp. 493–502, 1999.
[37] N. Vela, J. Fenoll, I. Garrido et al., "Photocatalytic mitigation of triazinone herbicide residues using titanium dioxide in slurry photoreactor," Catalysis Today, vol. 252, pp. 70–77, 2015.
[38] A. Adak, I. Das, B. Mondal et al., "Degradation of 2,4-dichlorophenoxyacetic acid by UV 253.7 and UV-H_2O_2: Reaction kinetics and effects of interfering substances," Emerging Contaminants, vol. 5, pp. 53–60, 2019.
[39] E. P. Melián, O. G. Díaz, J. D. Rodríguez, J. Araña, and J. P. Peña, "Adsorption and photocatalytic degradation of 2,4-dichlorophenol in TiO_2 suspensions. Effect of hydrogen peroxide, sodium peroxodisulphate and ozone," Applied Catalysis A: General, vol. 455, pp. 227–233, 2013.
[40] E. Kanchanatip, N. Grisdanurak, R. Thongruang, and A. Neramittagapong, "Degradation of paraquat under visible light over fullerene modified V-TiO_2," Reaction Kinetics, Mechanisms and Catalysis, vol. 103, no. 1, pp. 227–237, 2011.
[41] N. A. Eleburuike, W. A. Bakar, R. Ali, and M. F. Omar, "Photocatalytic degradation of paraquat dichloride over CeO_2-modified TiO_2 nanotubes and the optimization of parameters by response surface methodology," RSC Advances, vol. 6, no. 106, pp. 104082–104093, 2016.
[42] J. Yang, Q. Wu, S. He et al., "Completely <001> oriented anatase TiO_2 nanoarrays: topotactic growth and orientation-related efficient photocatalysis," Nanoscale, vol. 7, no. 33, pp. 13888–13897, 2015.
[43] D. Karimipourfard, R. Eslamloueyan, and N. Mehranbod, "Heterogeneous degradation of stabilized landfill leachate using persulfate activation by $CuFe_2O_4$ nanocatalyst: an experimental investigation," Journal of Environmental Chemical Engineering, vol. 8, no. 2, pp. 103426, 2020